Systems Science and Informatics Unit (SSIU)
Indian Statistical Institute, Bangalore
India

ESIEE
University of Paris-Est
France

19-22 October 2010
Bangalore

VISUALIZATION OF SPATIO-TEMPORAL BEHAVIOUR OF DISCRETE MAPS VIA GENERATION OF RECURSIVE MEDIAN ELEMENTS

B. S. Daya Sagar

Outline

- Mathematical Morphological Transformations employed include: Hausdorff Dilation, Hausdorff Erosion, Morphological Median Element Computation, and Morphological Interpolation.

Objectives

- To show relationships between the layers depicting noise-free phenomenon at two time periods.
- To relate connected components of layers of two time periods via FOUR possible categories of spatial relationships of THREE groups.
- To propose a framework to generate recursive interpolations via median set computations.
- To demonstrate the validity of the framework on epidemic spread.

VISUALIZATION OF SPATIO-TEMPORAL BEHAVIOR OF DISCRETE MAPS VIA GENERATION OF RECURSIVE MEDIAN ELEMENTS

(IEEE Transactions on Pattern Analysis and Machine Intelligence, v.31, no. 2, p. 378-384, 2010)

THREE Groups and FOUR categories??

- Three groups are conceived by checking the intersection properties between the corresponding connected components.
- Four categories under the above three groups are visualised via logical relationships and Hausdorff erosion and Haudorff dilation distances.
- What are these Hausdorff distances?
- What basics do we require to know to compute these distances?

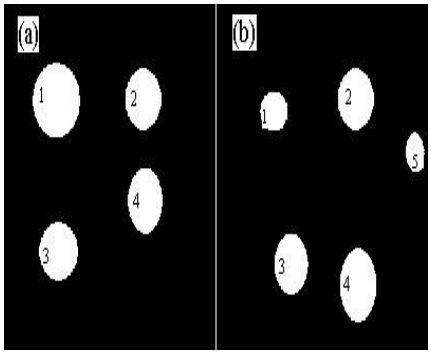

Basic Tools Required

BASIC MORPHOLOGIC TRANSFORMATIONS

Erosion and dilation are basic mathematical morphologic operators [16, 20]. These operations can be performed on any set X (a map in binary form) of the 2-dimensional Euclidean discrete space Z^2 by means of a structuring element B that is square in shape, symmetric about the origin, and has the primitive size 3 x 3. We explain these transformations including their multiscale versions.

The Minkowski erosion of X by B is the collection of all points x such that B_x when translated by x, is contained in the original set X, and is equivalent to the intersection of all the translates. Thus, the erosion of X by B is:

$$X \ominus B = \{x : B_x \subseteq X\} = \bigcap_{b \in B} X_{-b} \quad (1)$$

The Minkowski dilation of X by B is defined as the set of all points x, which the translated B_x intersects X, and is equivalent to the union of all translates:

$$X \oplus B = \{x : B_x \cap X \neq \varnothing\} = \bigcup_{b \in B} X_{-b} \quad (2)$$

The two morphological transformations Eqs. (1 & 2) can be performed by increasing the size of the structuring element to λB, where $\lambda = 0, 1, 2, \ldots, N$. The Reader may want to refer to [16, 20] for detailed explanations and implementations of these fundamental morphologic transformations along with their algebraic properties.

Hausdorff Erosion Distance and Hausdorff Dilation Distance

Let (X^t) and (X^{t+1}) be the non-empty compact sets at two time instants t and $t+1$. According to [13], the Hausdorff-erosion-distance $\sigma(X^t, X^{t+1})$ and the dilation-distance $\rho(X^t, X^{t+1})$ between X^t and X^{t+1} are defined respectively as:

$$\sigma(X^t, X^{t+1}) = \inf\left\{\lambda : \left[(X^t \ominus \lambda B) \subseteq X^{t+1}\right] or \left[(X^{t+1} \ominus \lambda B) \subseteq X^t\right]\right\} \quad (3)$$

$$\rho(X^t, X^{t+1}) = \inf\left\{\lambda : \left[X^t \subseteq (X^{t+1} \oplus \lambda B)\right] or \left[X^{t+1} \subseteq (X^t \oplus \lambda B)\right]\right\} \quad (4)$$

The Hausdorff dilation distance (introduced in [13]) is similar to the classic concept of "Hausdorff distance" [21]. Algebraically, these two distances yield metrics, which are dual to each other with respect to the "complement" operation.

The median set [13], which is central to the theme of the paper, can be computed by employing multiscale erosions and dilations along with certain logical operations. If there exists a bijection between the sets (X^t) and (X^{t+1})—such that (X^t) is completely contained in (X^{t+1}), $(X^t \subseteq X^{t+1})$—the equation for computing the median set $M(X^t, X^{t+1})$ between (X^t) and (X^{t+1}) takes the form:

$$M(X^t, X^{t+1}) = \bigcup_{\forall \lambda} \left((X^t \oplus \lambda B) \cap (X^{t+1} \ominus \lambda B) \right) \quad (5)$$

If (X^t) is only partially contained in (X^{t+1}), Eq. (5) takes the form:

$$M(X^t, X^{t+1}) = \bigcup_{\forall \lambda \geq 0} \left(\left[(X^t \cap X^{t+1}) \oplus \lambda B \right] \cap \left[(X^t \cup X^{t+1}) \ominus \lambda B \right] \right) \quad (6)$$

$M(X^t, X^{t+1})$ satisfies a more symmetrical property (see [13, 22]):

$$\mu = \inf \left\{ \lambda : \lambda \geq 0, (X^t \ominus \lambda B) \supseteq (X^{t+1} \ominus \lambda B) \right\} = \rho(X^t, M) = \sigma(M, X^{t+1}) \quad (7)$$

$M(X^t, X^{t+1})$ is at Hausdorff dilation distance μ from (X^t), while $M(X^t, X^{t+1})$ is at Hausdorff erosion distance μ from (X^{t+1}). This further implies, for the case of $(X^t \subseteq X^{t+1})$, that $X^t \subseteq M \subseteq X^{t+1}$, and one has strictly

$$\rho(X^t, M) = \inf_{\forall \lambda \geq 0} \left\{ \lambda : M \subseteq (X^t \oplus \lambda B) \right\}$$ and

$$\sigma(M, X^{t+1}) = \inf_{\forall \lambda \geq 0} \left\{ \lambda : (X^{t+1} \ominus \lambda B) \subseteq M \right\}.$$

Limited Layered Sets

The layered information depicting a specific phenomenon available for static systems or for a time-dependent (dynamic) system can be of three types: ordered, semi-ordered, or disordered. Let (X^t) and (X^{t+1}) be connected components (e.g. lakes) at time periods 't' and 't+1' represented on Z^2 (Fig. 1. a,b). For notational simplicity, we denote (X^t) and (X^{t+1}) as sets (layers) and represent the connected components and as their subsets. and , , are assumed always to be non-empty and compact. In what follows, "sets" and "layered data", as well as "subsets" and "connected components", are interchangeably used.

Spatial Relationships Between Sets and Their Categorization

Ordered sets.

semi-ordered sets, if subsets of X^t (resp. X^{t+1}) are only partially contained in the other set X^{t+1} (resp. X^t).

Whereas, (X^t) and (X^{t+1}) are considered as *disordered sets* if there exists an empty set while taking the intersection of (X^t) and (X^{t+1}) (or) of their corresponding subsets.

Description of categories via logical relations

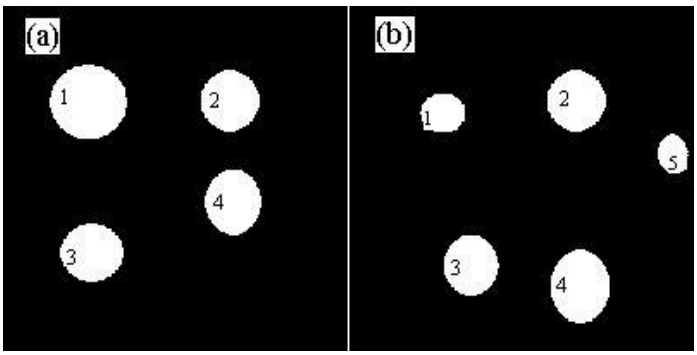

Description of categories via logical relations

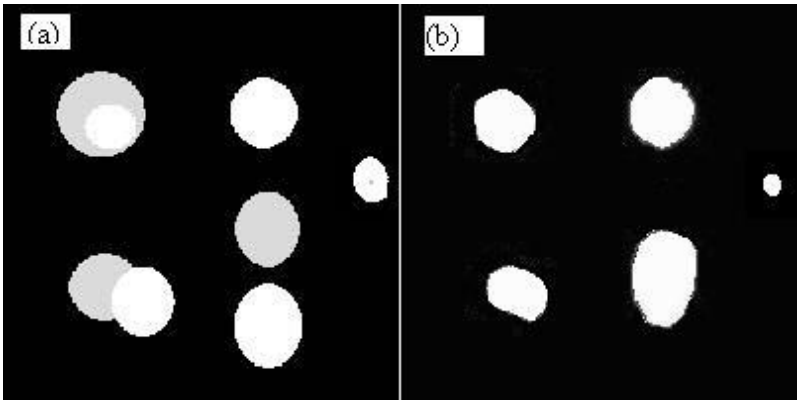

Categories via Hausdorff Erosion and Dilation Distances

TABLE 1. CATEGORY-WISE HAUSDORFF DISTANCES

Group	Category	$\sigma\left(X_i^t, X_i^{t+1}\right)$	$\rho\left(X_i^t, X_i^{t+1}\right)$
I	1	0	0
I	2	≥ 1	≥ 1
II	3	Does not exist	≥ 1
III	4	Does not exist	Does not exist

Investigation of Time-varying Phenomena

- Interpolation is a technique used to generate intermediary images between the initial and final images (Beucher, 1998).
- Various tools are available to create interpolation, including classical arithmetic interpolation, morphing techniques, and weighting functions.
- However, morphological interpolation is adopted here as it better preserves the topological (connectivity) properties of the images (Mathematical Morphology and Image Interpolation (No date). *The Image Interpolation Page* [Online]).
- Iwanowski and Serra (1999) defined morphological interpolation between two sets (e.g., set *X* and set *Y*) as,

$$M(X,Y) = \{(X \oplus B)(Y \ominus B)\}$$

13

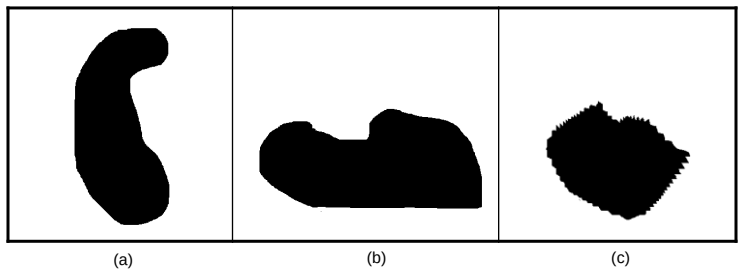

An example of morphological interpolation. (a) Initial set X, (b) final set Y, and (c) resultant interpolated set of X and Y.

14

Investigation of Time-varying Phenomena

- From Iwanowski (2007), the interpolated sequence of fractal sets between M_1 and $M_{I=16}$ is obtained by iterative generation of new morphological sets, as shown below:

1st iteration:

$M_8 = M(M_1, M_{16})$

2nd iteration:

$M_4 = M(M_1, M_8)$

$M_{12} = M(M_8, M_{16})$

3rd iteration:

$M_2 = M(M_1, M_4)$

$M_6 = M(M_4, M_8)$

$M_{10} = M(M_8, M_{12})$

$M_{14} = M(M_{12}, M_{16})$

4th iteration:

$M_3 = M(M_2, M_4)$

$M_5 = M(M_4, M_6)$

$M_7 = M(M_6, M_8)$

$M_9 = M(M_8, M_{10})$

$M_{11} = M(M_{10}, M_{12})$

$M_{13} = M(M_{12}, M_{14})$

$M_{15} = M(M_{14}, M_{16})$

15

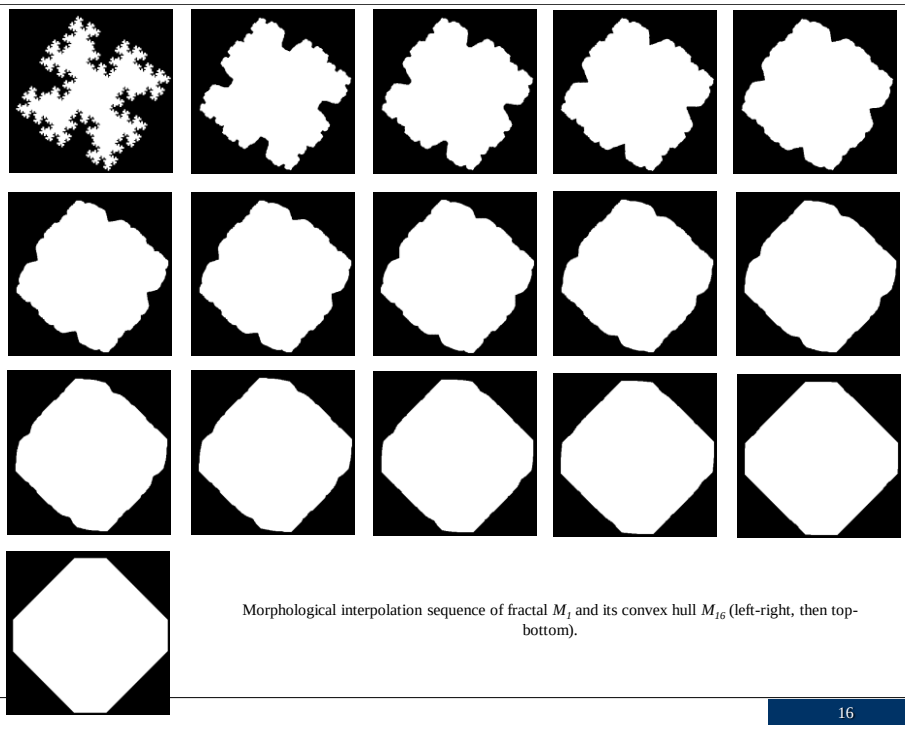

Morphological interpolation sequence of fractal M_1 and its convex hull M_{16} (left-right, then top-bottom).

16

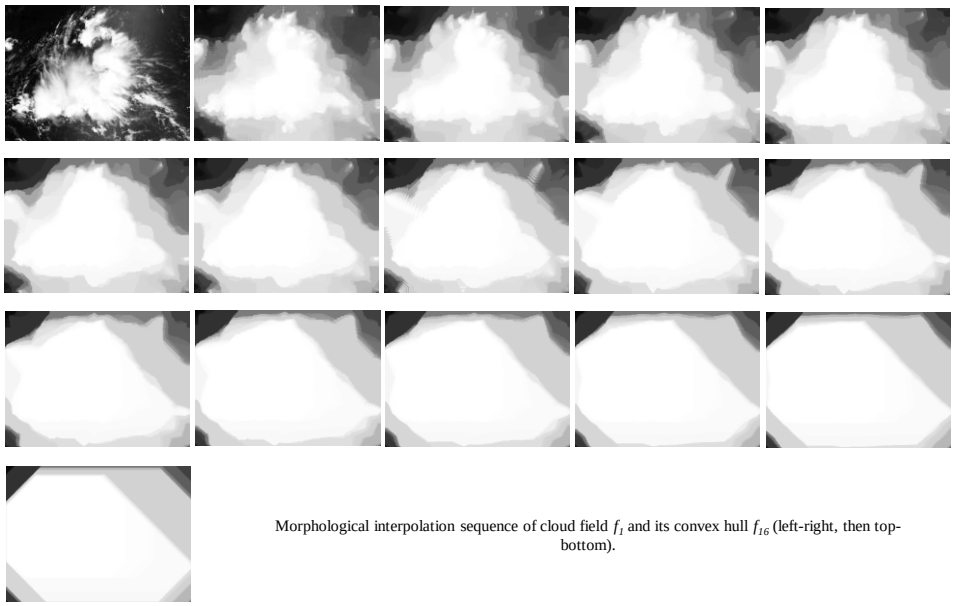

Morphological interpolation sequence of cloud field f_1 and its convex hull f_{16} (left-right, then top-bottom).

17

Interpolated Sequence of Lakes' Data of Two Seasons

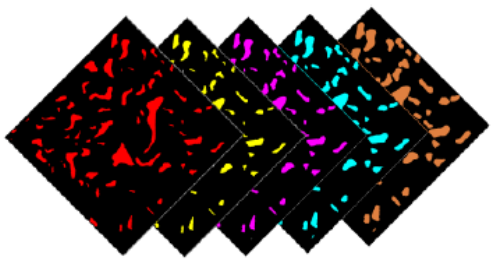

Fig. 4. A sequence of interpolated sets (slices) in between the two input slices shown in Figs. 3a, b. Equations 8(a) and 14 are used to recursively generate the interpolated slices. The layer depicting water bodies with magenta color is the median set shown in Fig. 3c.

Observed and Interpolated Epidemic Spread Maps

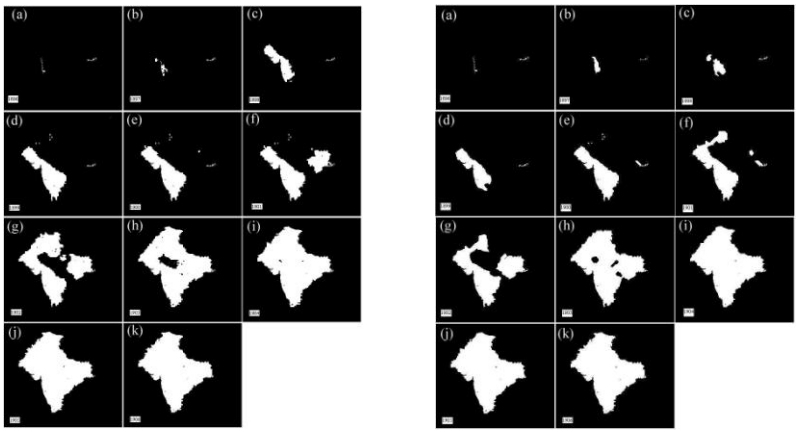

Observed and Interpolated Sequences

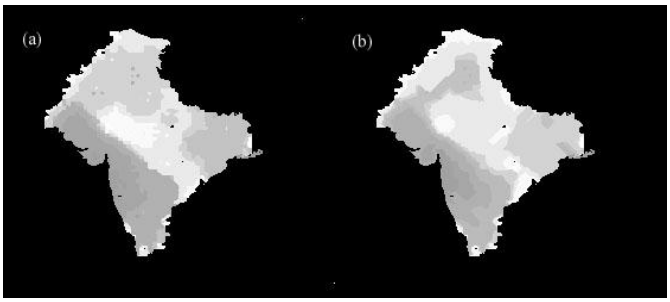

Validation

TABLE 2. μ VALUES COMPUTED FOR X^t AND X^{t+1} AND X^t AND X^{t+2}

t, t+1, t+2	μ	
	$M\left(X^t, X^{t+1}\right)$	$M\left(X^t, X^{t+2}\right)$
1896, 1897, 1898	3	9
1897, 1898, 1899	9	15
1898, 1899, 1900	11	11
1899, 1900, 1901	2	12
1900, 1901, 1902	12	15
1901, 1902, 1903	13	16
1902, 1903, 1904	9	14
1903, 1904, 1905	7	7
1904, 1905, 1906	2	2
1905, 1906, -	1	-

TABLE 3. HAUSDORFF DISTANCE VALUES

t	$\rho\left[M\left(X^t, X^{t+1}\right), X^{t+2}\right]$	$\sigma\left[M\left(X^t, X^{t+1}\right), X^{t+1}\right]$	$\rho\left(X^t, X^{t+1}\right)$	$\sigma\left(X^t, X^{t+1}\right)$
1896	8	2	7	1
1897	2	2	1	1
1898	1	1	1	1
1899	4	2	1	1
1900	12	9	1	1
1901	8	7	2	1
1902	8	8	1	1
1903	3	3	2	1
1904	2	2	1	1
1905	-	-	2	1

Animation of Epidemic Spread

http://www.isibang.ac.in/~bsdsagar/Epid-animate2.avi

Additional (Results) Illustrations

1) Cloud field segmentation via multiscale convexity analysis
2) Generation of geodesic flow fields
3) Visualization of rock porous medium, pore channel, pore throats, and pore bodies

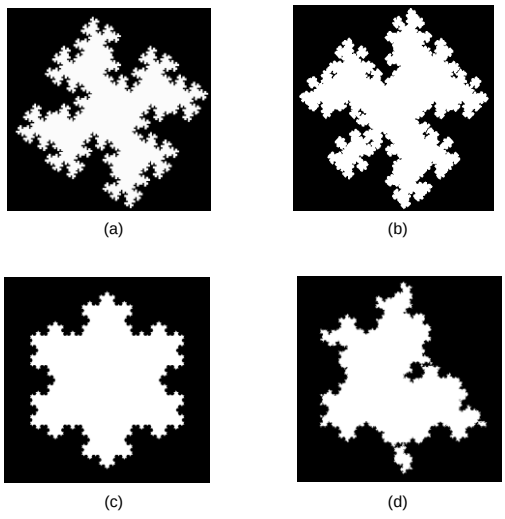

(a) Koch Quadric fractal, (b) random Koch Quadric fractal, (c) Koch Triadic fractal, and (d) random Koch Triadic fractal.

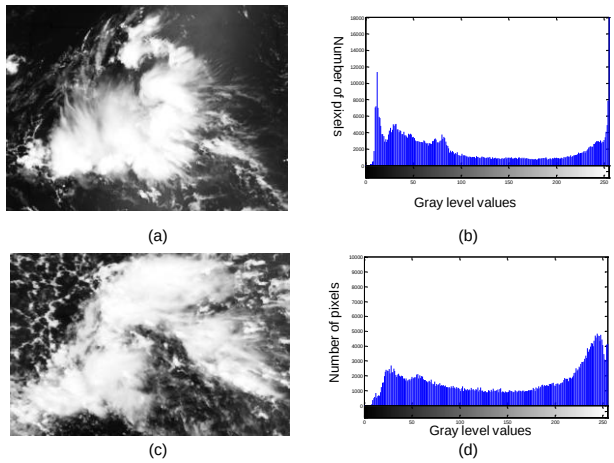

(a) isolated MODIS cloud (cloud-1), (b) histogram of (a), (c) isolated MODIS cloud (cloud-2), and (d) histogram of (c).

25

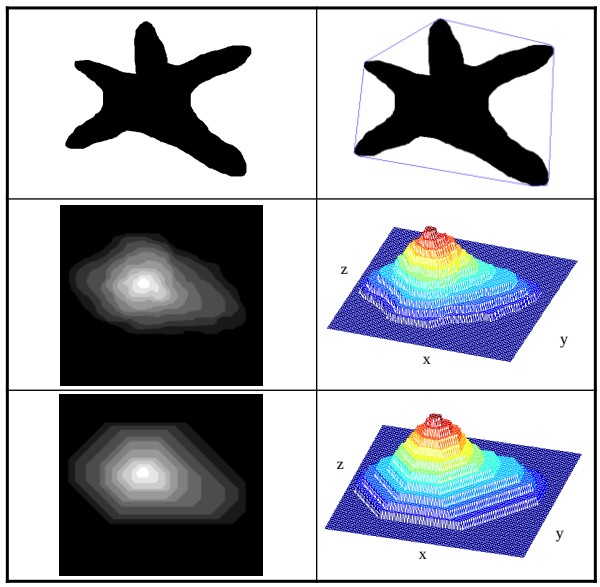

(a) A threshold set decomposed from a synthetic cloud function, (b) convex hull of a threshold set shown in (a), (c) a synthetic cloud function consists of 10 gray levels – which can be decomposed maximally into 10 threshold sets, (d) 3D representation of synthetic cloud function (c), (e) convex hull of (c)

26

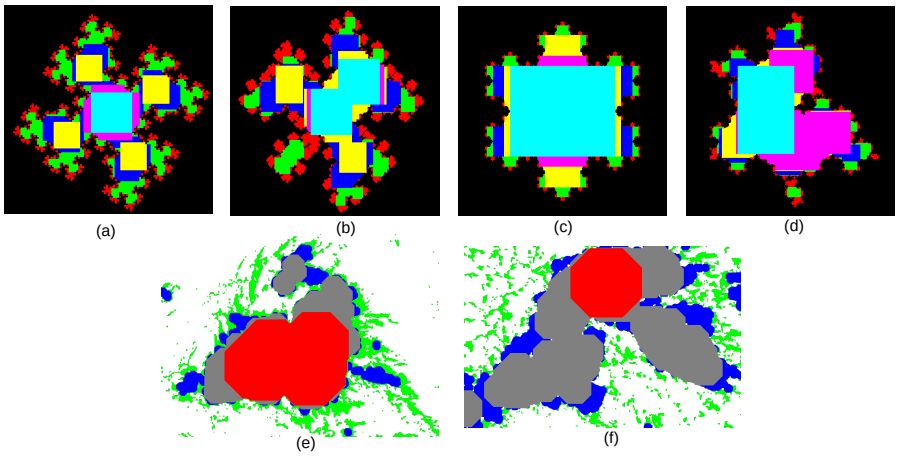

Six zones segmented from deterministic and random Koch Quadric and Koch Triadic fractals, and (e, f) Four zones segmented from realistic MODIS clouds.

- Each of the segmented six zones from fractals, and each of the four zones partitioned from cloud fields evidently possess different degrees of spatial complexity measures. A simple framework is provided here to compute the complexity measure of each segmented zone.

27

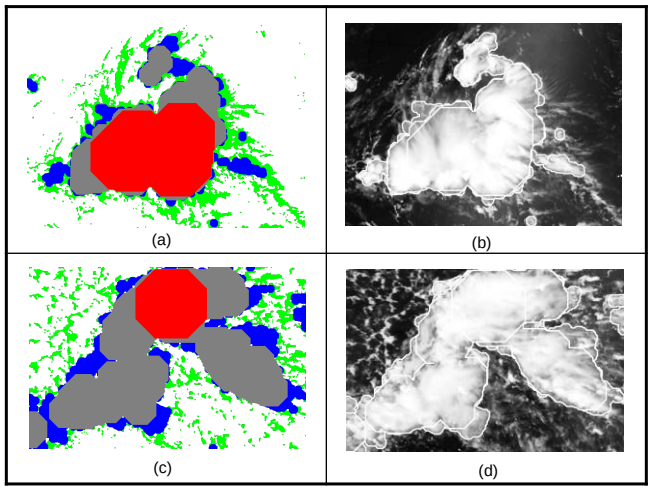

(a) Colour-coded binarized (by choosing threshold gray level value 128) cloud-images at three threshold-opening cycles superimposed on binarized original cloud-1 colour-coded with green, (b) boundaries of 12th, 32nd, and 100th opened cloud-1 images and thresholded original cloud-1 superimposed on the original cloud image, (c) colour-coded binarized (by choosing a threshold gray level value 110) cloud-2 images at threshold-opening cycles superimposed on binarized cloud-2 colour-coded with green, and (d) boundaries of 12th, 49th, and 100th opened cloud-2 images and thresholded original cloud-2

28

Geodesic Flow Fields and Spectrum of Discrete Functions

- A framework to derive flow fields and spectrum in discrete functions particularly in digital topographic basins and cloud field is presented.
- Hereafter, "basin" refers to inland, tidal, floodplain, coastal, estuary regions, and digital topographies which include DEMs and DBMs, and "topography" refers to both surficial and bottom topographies.
- Through analysis of flow fields that are simulated via geodesic morphology, a new descriptor is generated that characterizes such discrete functions.
- This framework is demonstrated on (i) three synthetic basins, (ii) one realistic DEM, (iii) one realistic DBM, and (iv) two MODIS cloud fields.
- This study provides potentially invaluable insights to further investigate the travel-time flood propagation within basins of both fluvial and tidal systems, as well as the travel-time field and flow perturbations in cloud.

29

Geodesic Flow Fields and Spectrum of Discrete Functions

- Computation of this new descriptor involves the following five steps:

(i) basin or cloud field in digital form representing topographic fluctuations or height

(ii) hierarchical threshold decomposition of

(iii) proper indexing of these sets to determine the marker

(iv) perform geodesic [illegible]

(v) finally to generate a new descriptor—geodesic spectrum to characterize basin or cloud

30

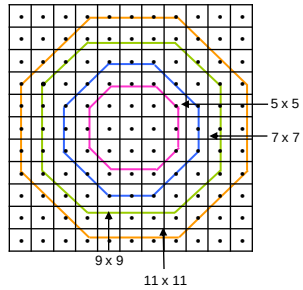

Octagonal symmetric structuring elements of various primitive sizes ranging from 5 × 5 to 11 × 11. These primitive sizes can be considered as B in the employed equations to simulate flow fields with various velocities.

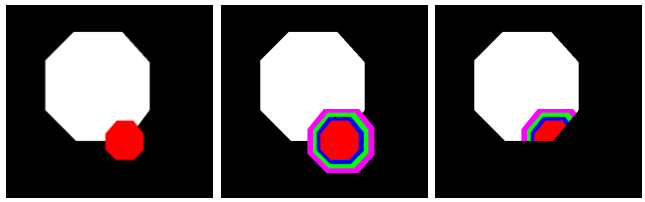

(a) Marker set S_i (in red) and mask set S_{i+1} (in white), (b) after iterative dilations up to fourth level superposed on the mask set S_{i+1}, and (c) the dilated marker set of four iterations intersected with mask set S_{i+1}.

31

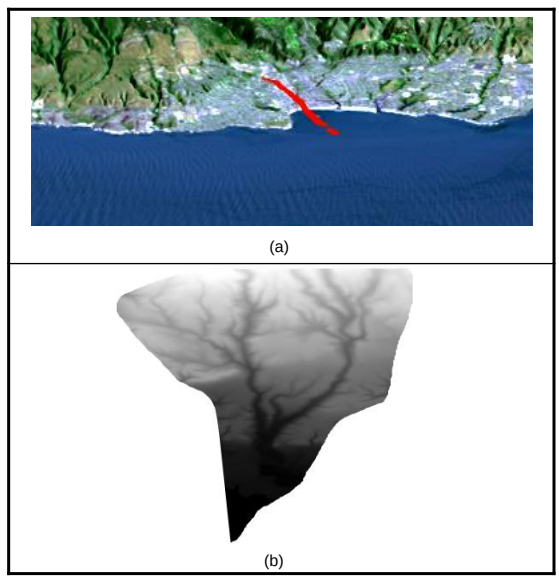

(a) 3D view of Santa Cruz, and (b) Digital elevation map of Santa Cruz.

32

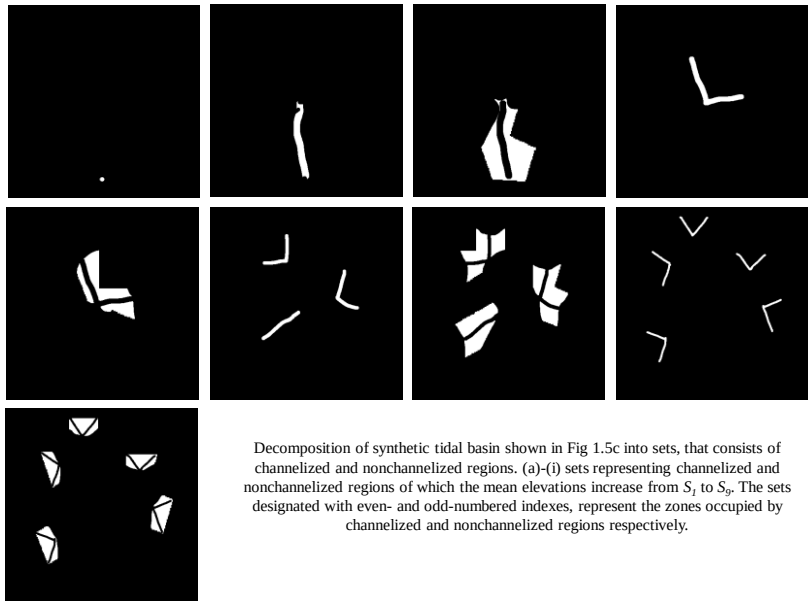

Decomposition of synthetic tidal basin shown in Fig 1.5c into sets, that consists of channelized and nonchannelized regions. (a)-(i) sets representing channelized and nonchannelized regions of which the mean elevations increase from S_1 to S_9. The sets designated with even- and odd-numbered indexes, represent the zones occupied by channelized and nonchannelized regions respectively.

33

Geodesic Flow Fields and Spectrum of Discrete Functions

- Geodesic morphological transformations (Lantuejoul and Maisonneuve, 1984) are adopted to simulate flow field propagation in discrete functions like basin and cloud field.
- James Sethian's (1999) level set theory and Jean Serra's (1982) random sets and mathematical morphologic concepts offer various transformations to simulate flow fields within basin with physical viability.
- To implement geodesic transformations, the basin is considered as a mask, and the inlet point (through which water flows into the basin during the high flood) is taken as a marker from which the flow propagates into the basin as the flood level increases.

34

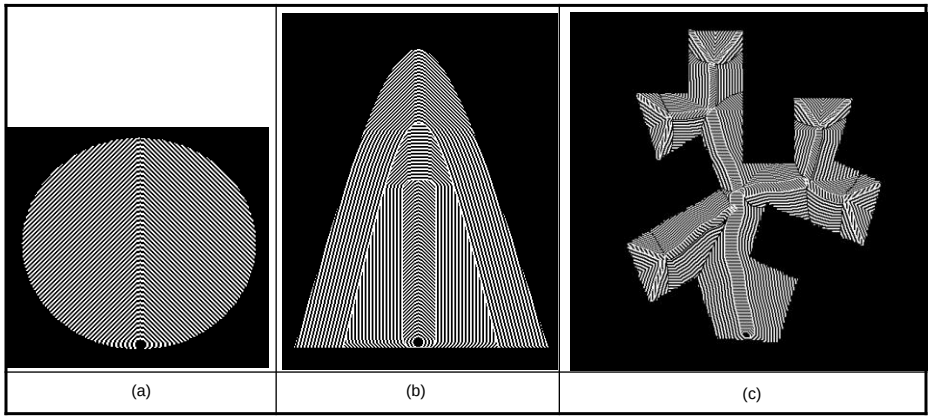

(a) Flow fields with isotropic propagation, (b) isotropic flow fields, and orthogonality between the flow fields of channelized and nonchannelized zones is obvious, and (c) flow fields within the tidal basin.

35

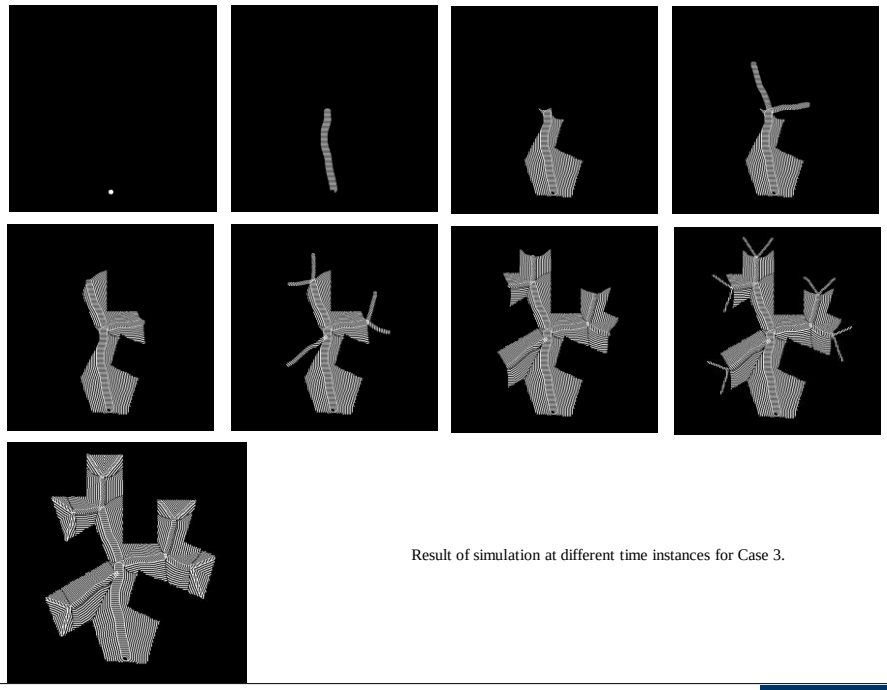

Result of simulation at different time instances for Case 3.

36

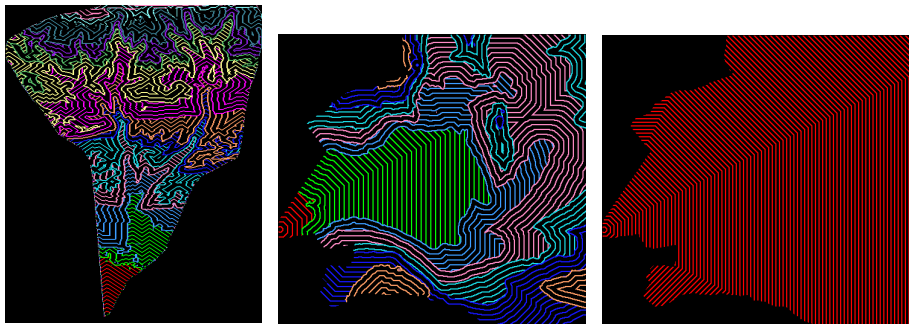

(a) (b) (c)

(a) Flow field simulated on Santa Cruz DEM by using octagon structuring element, (b) flow field simulated on San Francisco Bay bathymetry by using octagon structuring element, and (c) flow field simulated on San Francisco Bay without considering bathymetry.

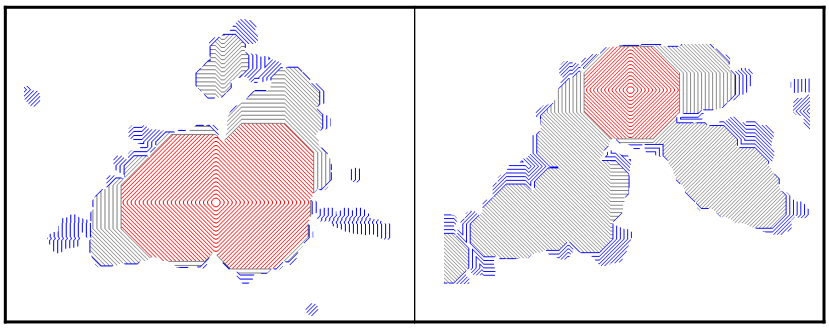

(a) (b)

(a) Simulated flow fields of MODIS cloud-1, and (b) simulated flow fields of MODIS cloud-2.

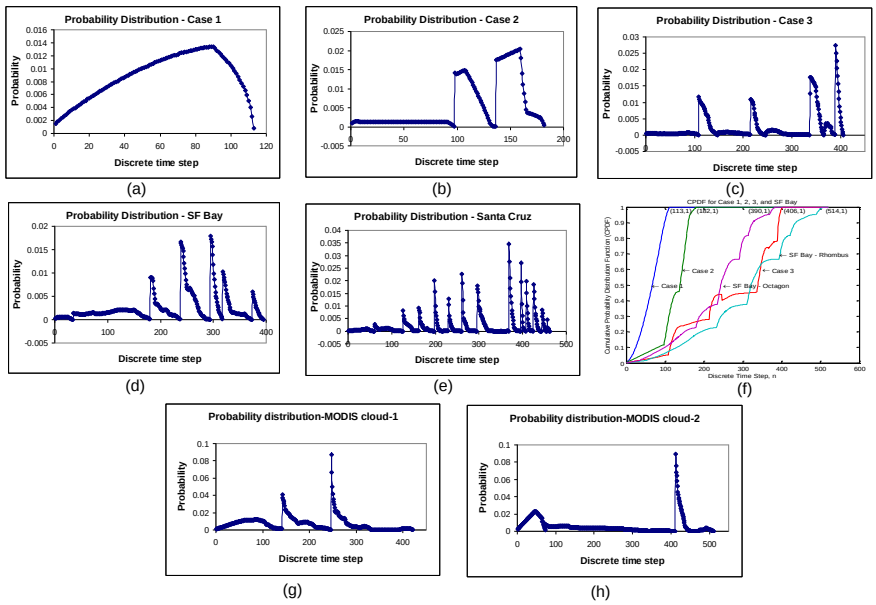

Figure. Probability of estimated area flooded/propagated at each discrete time step.

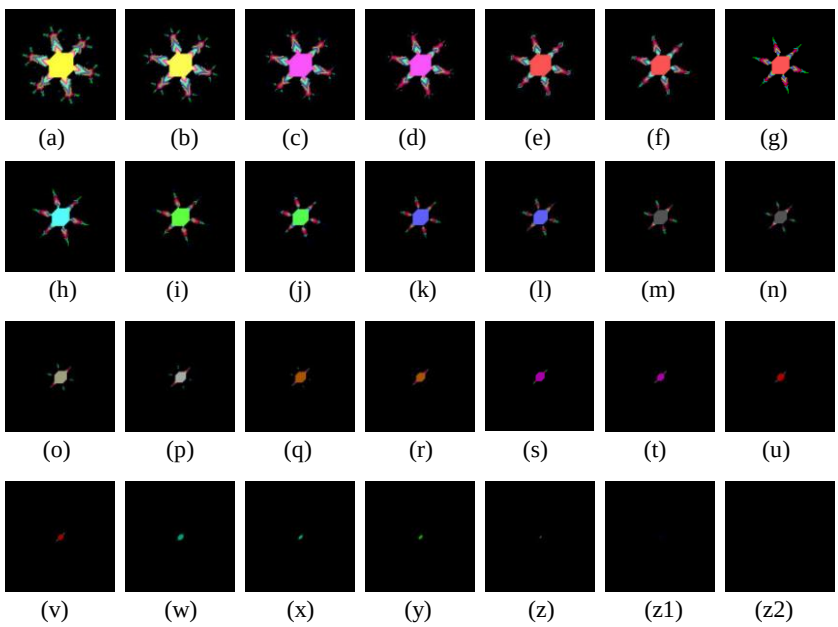

Figure : Extracting pore throat from eroded **triadic Koch curve** images by structuring element of octagon.

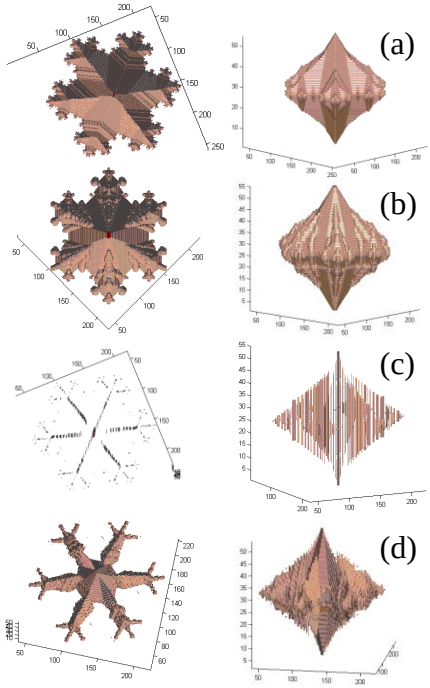

Top and side views of 3D model at

(a) binary pore,

(b) pore-bodies,

(c) pore-channel, and

(d) pore-throat

of **triadic Koch curve**

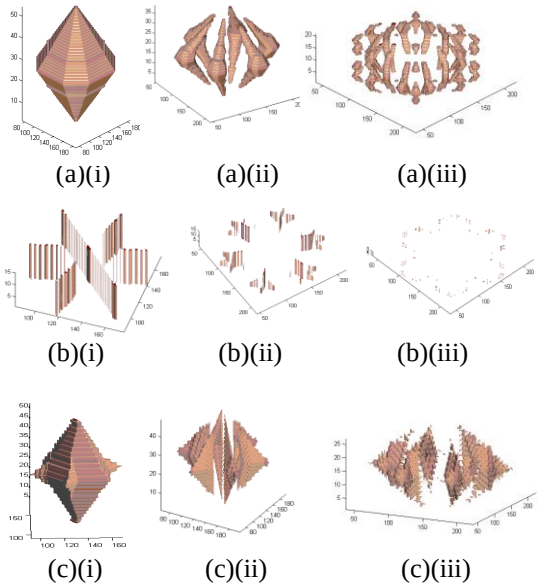

The diagram shows the order-wise isolated 3D pore quantities at (i) inner, (ii) middle and (iii) outer layers of

(a) pore bodies,

(b) pore channels, and

(c) pore throats.

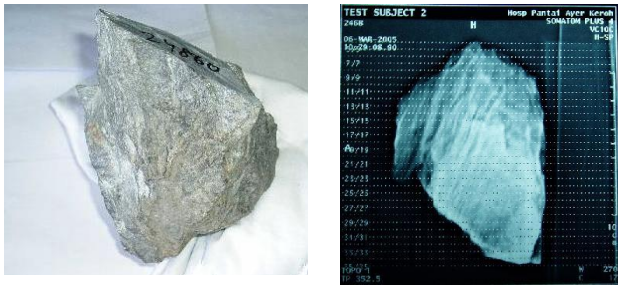

(a) (b)

(a) The photograph of schist rock sample; (b) the CT scans applied at schist rock sample

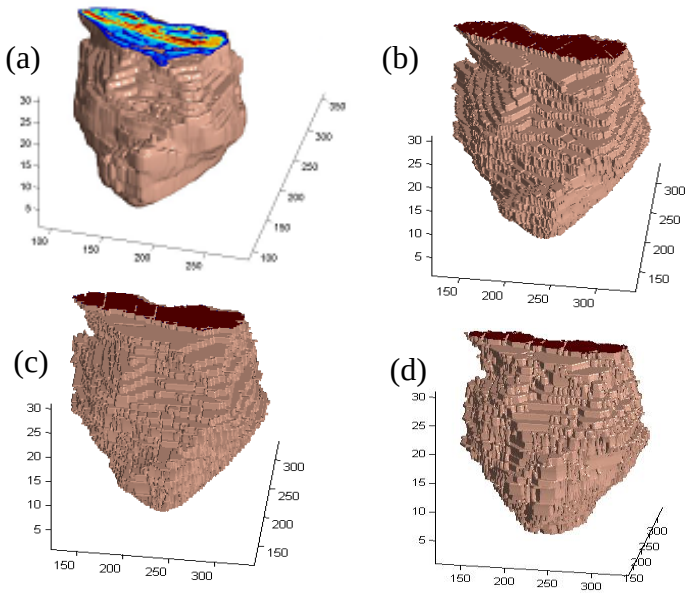

The 3D reconstruction of (a) binary schist image; non-overlapping decomposition technique by structuring elements of (b) rhombus, (c) square and (d) octagon

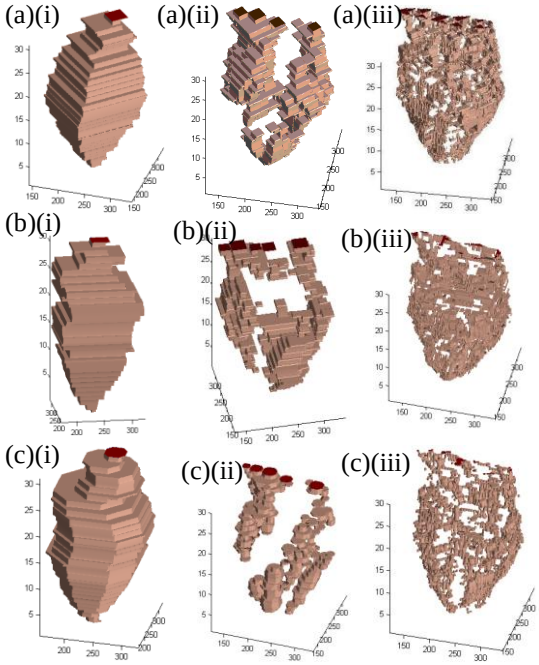

Order-wise isolated 3D rock quantities at (i) inner, (ii) middle and (iii) outer layers rock by structuring elements

(a) rhombus

(b) square, and

(c) octagon.

Acknowledgments: Grateful to collaborators, mentors, reviewers, examiners, and doctoral students—Prof. S. V. L. N. Rao, Prof. B. S. P. Rao, Dr. M. Venu, Mr. Gandhi, Dr. Srinivas, Dr. Radhakrishnan, Dr. Lea Tien Tay, Dr. Chockalingam, Dr. Lim Sin Liang, Dr. Teo Lay Lian, Prof. Jean Serra, Prof. Gabor Korvin, Prof. Arthur Cracknell, Prof. Deekshatulu, Prof. Philippos Pomonis, Prof. Peter Atkinson, Prof. Hien-Teik Chuah and several others.